Nanoscale

PAPER

View Article Online
View Journal | View Issue

Cite this: *Nanoscale*, 2016, **8**, 13513

Size-dependent, stochastic nature of lipid exchange between nano-vesicles and model membranes†

Seyed R. Tabaei,[a,b] Jurriaan J. J. Gillissen,[a,b] Setareh Vafaei,[a,b] Jay T. Groves[c] and Nam-Joon Cho*[a,b,d]

Received 11th May 2016,
Accepted 13th June 2016

DOI: 10.1039/c6nr03817d

www.rsc.org/nanoscale

The interaction of nanoscale lipid vesicles with cell membranes is of fundamental importance for the design and development of vesicular drug delivery systems. Here, we introduce a novel approach to study vesicle–membrane interactions whereby we are able to probe the influence of nanoscale membrane properties on the dynamic adsorption, exchange, and detachment of vesicles. Using total internal reflection fluorescence (TIRF) microscopy, we monitor these processes in real-time upon the electrostatically tuned attachment of individual, sub-100 nm vesicles to a supported lipid bilayer. The observed exponential vesicle detachment rate depends strongly on the vesicle size, but not on the vesicle charge, which suggests that lipid exchange occurs during a single stochastic event, which is consistent with membrane stalk formation. The fluorescence microscopy assay developed in this work may enable measuring of the probability of stalk formation in a controlled manner, which is of fundamental importance in membrane biology, offering a new tool to understand nanoscale phenomena in the context of biological sciences.

Nano-sized lipid vesicles have attracted considerable attention in nano-biotechnology and nano-medicine as carriers for delivery of drugs, genes and imaging agents, due to their biocompatibility and their ability to be functionalized with a wide range of targeting and trafficking moieties.[1–3] Several mechanisms have been postulated by which vesicles can interact with cells including adsorption, endocytosis, fusion and lipid exchange.[4] The lipid exchange involves spontaneous intermembrane lipid transfer between the vesicle and the cell membrane. Exchange of lipids and their precursors also occurs between biomembranes and plays a key role in lipid metabolism and signaling, membrane lipid organization, drug function and many other biological processes.[2,5–7] Lipid transfer between cellular membranes occurs either through the so-called vesicular transport in which large amounts of lipids are transferred *via* protein-mediated fusion of vesicles that bud from a donor compartment with a target membrane[8] or through non-vesicular transport[9] by lipid transfer proteins (LTPs)[10] that shuttle lipid monomers between membranes. Spontaneous intermembrane lipid transfer has also been observed in protein free systems.

Mechanistically, the spontaneous lipid transfer may occur through transfer of individual lipids from one membrane into another by diffusion through the aqueous medium[11] (Fig. 1a). The time scale of phospholipid transfer *via* lipid diffusion however is shown to be on the order of hours[11,12] and thus has less physiological relevance. For short intermembrane separations, *e.g.* for adhering membranes or for transient membrane collisions, lipids may directly transfer between the apposing membranes without exposure to the aqueous medium[13,14] (Fig. 1b). Alternatively, under these conditions, lipid transfer may occur upon the re-organization of the membrane structure into a short-lived "hemi-fused" state, where the two proximal leaflets form a local, neck-like connection, also called a membrane stalk[15–17] (Fig. 1c). A stalk is a transient state, which upon formation results in a rapid lipid exchange between the opposing membranes through lateral lipid diffusion in the connected leaflets.[18]

In this work we study the transfer of lipids between nano-sized vesicles and model lipid membranes. The aim of this work is to decipher the dominant mechanism for the exchange, being either transfer of individual lipids in many steps or the transfer of many lipids in one or a few steps as an effect of stalk formation. We focus on exchange between membranes that are brought into close contact. The close contact

[a]*School of Materials Science and Engineering, Nanyang Technological University, 50 Nanyang Avenue 639798, Singapore. E-mail: njcho@ntu.edu.sg*
[b]*Centre for Biomimetic Sensor Science, Nanyang Technological University, 50 Nanyang Drive 637553, Singapore*
[c]*Department of Chemistry, University of California, Berkeley, California 94720, USA*
[d]*School of Chemical and Biomedical Engineering, Nanyang Technological University, 62 Nanyang Drive 637459, Singapore*
†Electronic supplementary information (ESI) available. See DOI: 10.1039/c6nr03817d

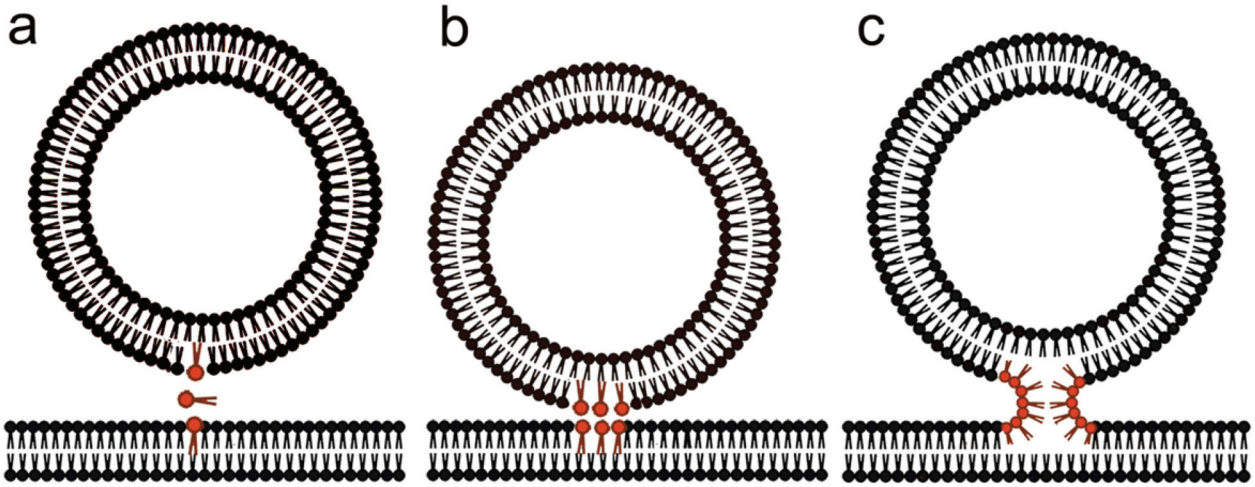

Fig. 1 Schematic illustration of three possible mechanisms for spontaneous lipid exchange between a vesicular and a planar bilayer. (a) Lipid monomers desorb from one bilayer and diffuse through an aqueous medium to insert into a different bilayer. (b) Lipid monomers transfer directly between membranes without exposure to aqueous medium. (c) Lipid transfer *via* membrane stalk formation occurs through lateral diffusion along the merged leaflets of the opposing membranes.

between membranes can be established by nonspecific interactions,[19] such as electrostatic charge on membrane surfaces,[20–23] or forces due to solute depletion in the intermembrane hydration layer.[24]

Earlier studies on spontaneous (non-protein-mediated) inter-membrane lipid transfer have been primarily focused on suspended vesicles in bulk.[19] However, measurements on the interaction of a collection of suspended vesicles are usually convoluted by vesicle aggregation and/or fusion. In addition, generally, data obtained from ensemble average measurements provide limited insight into the underlying mechanisms. To overcome these limitations, a range of assays, based on the microscopy imaging of surface adhering vesicles, have been developed for a range of studies, including vesicle fusion,[25] membrane transport,[26,27] protein/peptide–membrane interaction[28–30] and membrane active enzymes.[31]

Here we develop a total internal reflection fluorescence microscopy-based assay to decipher which mechanism (transfer of individual lipids or stalk formation) is predominantly responsible for spontaneous lipid transfer between small unilamellar vesicles (SUVs) and supported lipid bilayers (SLBs). We do this by studying the desorption rate of electrostatically adhering SUVs as a function of the vesicle size, fluidity and charge. Indeed the membrane curvature (vesicle size), lipid composition and membrane phase state affect the various interface-specific properties of membranes such as molecular recognition in interfacial environments,[32,33] action of membrane active enzymes[31] and peptides[28] as well as membrane fusion.[34]

The SLB has widely been used as a model for biological membranes.[35,36] Processes occurring at the SLB interface can be monitored by a range of surface sensitive techniques, such as the quartz crystal micro-balance,[37] surface plasmon resonance[38] and total internal reflection fluorescence (TIRF). TIRF in particular is a versatile tool for studying interfacial events at sensitivity down to the level of single molecules.[39] We use TIRF microscopy to observe fluorescently labeled SUVs which are electrostatically adhering to the SLB. The microscopy images provide the size of individual vesicles and their residence times on the SLB, revealing, among other things, insights into the effect of membrane curvature on the lipid exchange between the SUVs and the SLB.

Negatively charged and fluorescently labeled SUVs were prepared using the extrusion method, with a size of approximately 100 nm, which is similar to that of inter-cellular cargo vesicles.[40] We study three types of fluid-phase SUVs that are composed of zwitterionic (neutrally charged) DOPC (1,2-dioleoyl-*sn-glycero*-3-phosphocholine) lipids, mixed with 1 mol% fluorescent rhodamine-PE [1,2-dioleoyl-*sn-glycero*-3-phosphoethanolamine-*N*-(lissamine rhodamine B sulfonyl)] lipids and with 1 mol%, 5 mol% or 50 mol% anionic (negatively charged) DOPS (1,2-dioleoyl-*sn-glycero*-3-phospho-L-serine) lipids. In addition we also study one type of gel-phase SUV that is composed of zwitterionic DPPC (1,2-dipalmitoyl-*sn-glycero*-3-phosphocholine) lipids mixed with 1 mol% rhodamine-PE lipids and with 5 mol% anionic DOPS lipids. These DPPC vesicles are in the gel-phase as the gel-to-liquid phase transition temperature of DPPC is about 41 °C,[41] while the experiment was conducted at room temperature.

Positively charged and fluorescently labeled SLBs were formed on the glass wall of a fluidic chamber, using the vesicle fusion method. For this purpose positively charged and fluorescently labeled SUVs were fabricated by the extrusion method, composed of zwitterionic DOPC lipids mixed with 10% cationic (positively charged) DOEPC (*sn-glycero*-3-ethylphosphocholine) lipids. The fluidity of the SLB is confirmed by the fluorescence recovery after photobleaching (FRAP) method as shown in Fig. 2a. After photobleaching, the lateral

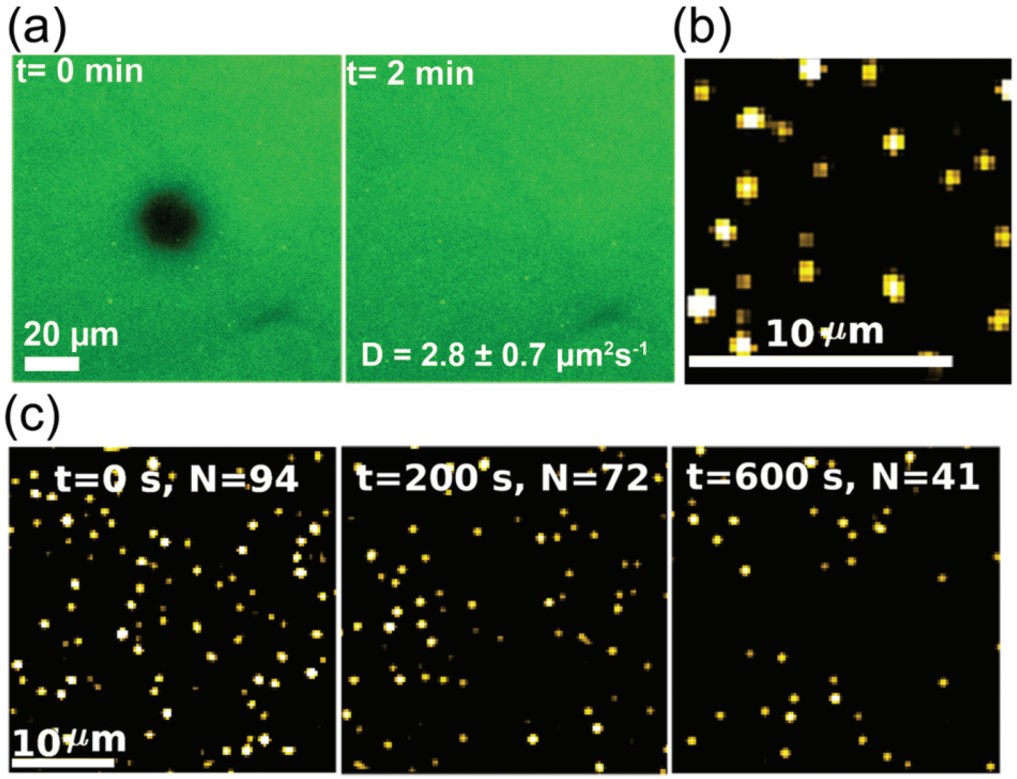

Fig. 2 Monitoring the detachment of individual nano-sized, anionic, lipid vesicles [DOPC : DOPS, (95 : 5)], which are electrostatically adhering to a fluid, cationic, supported lipid bilayer (SLB) [DOPC : DOEPC, (90 : 10)]. (a) Fluorescence micrographs of the SLB, immediately after photobleaching (left) and after two minutes of recovery (right). The intensity fully recovers, indicating that the lipids are laterally mobile. (b) Total internal reflection fluorescence (TIRF) microscopy image, resolving individual vesicles as diffraction-limited spots. (c) TIRF images at three time instances during a time period of 10 min, showing that the vesicles detach from the SLB over time. In the experiment 100 images of 136 × 136 μm were acquired at 20 s time intervals. (b) and (c) show a fraction of the TIRF images for clarity.

lipid diffusivity is determined from the time evolution of the fluorescence intensity profile (see ESI Fig. S1†), giving $D = 2.8 \pm 0.7\ \mu m^2\ s^{-1}$, which is in good agreement with previous reports.[42]

After SLB formation, the negatively charged and fluorescently labeled SUVs were injected into the fluidic chamber, where they electrostatically adhere to and diffuse on the positively charged SLB surface (see ESI Video S1†). Subsequent exchange of charged lipids between the SUVs and the SLB may lead to SUV charge equilibration and subsequent SUV desorption. In the present work we measure this SUV desorption using total internal reflection fluorescence (TIRF) microscopy. In the experiment we ensure a low SUV surface coverage (~1 vesicle per 10 μm^2), such that the charge exchange is negligible with respect to the total SLB charge, which therefore may be considered unaffected by the charge transfer between the SUVs and the SLB. The low surface coverage furthermore allows observing individual vesicles as diffraction-limited spots in the TIRF images (Fig. 2b).

Fig. 2c shows typical TIRF micrographs of membrane-attached vesicles at three time instances. After the initial attachment, the total number of vesicles is observed to decrease over time, indicating that vesicles spontaneously detach from the bilayer. Kunze *et al.* measured in a similar system the time dependent vesicle attachment and detachment using the quartz crystal microbalance with dissipation monitoring (QCM-D) method.[43] They also measured the corresponding lipid composition of the bilayer at each step using time-of-flight secondary ion mass spectrometry.[44] This provided evidence for extensive lipid transfer between the initial SLB and the oppositely charged SUVs, indicating that detachment occurs after charge neutralization of the SUVs due to lipid exchange between the two interacting membranes.

Fig. 3a shows the kinetics of vesicle detachment (for the four cases studied) *via* the number of detected vesicles N, normalized with the value at $t = 0$ (directly after adsorption), on a logarithmic y-axis, as a function of time. In each case, the linear time dependence of $\log(N)$ corresponds to an exponential decay, *i.e.* $dN/dt = -kN$. The fitted detachment rate $k \sim 10^{-3}\ s^{-1}$ (see ESI Table S1† for vesicle detachment rates, compositions and sizes) is in the same range as the values measured in similar systems, using the QCM-D technique.[43,45] Surprisingly, Fig. 3a shows that the detachment rate is (nearly) unaffected by the vesicle charge density for vesicles containing 1 mol%, 5 mol% and 50 mol% negatively charged lipids.

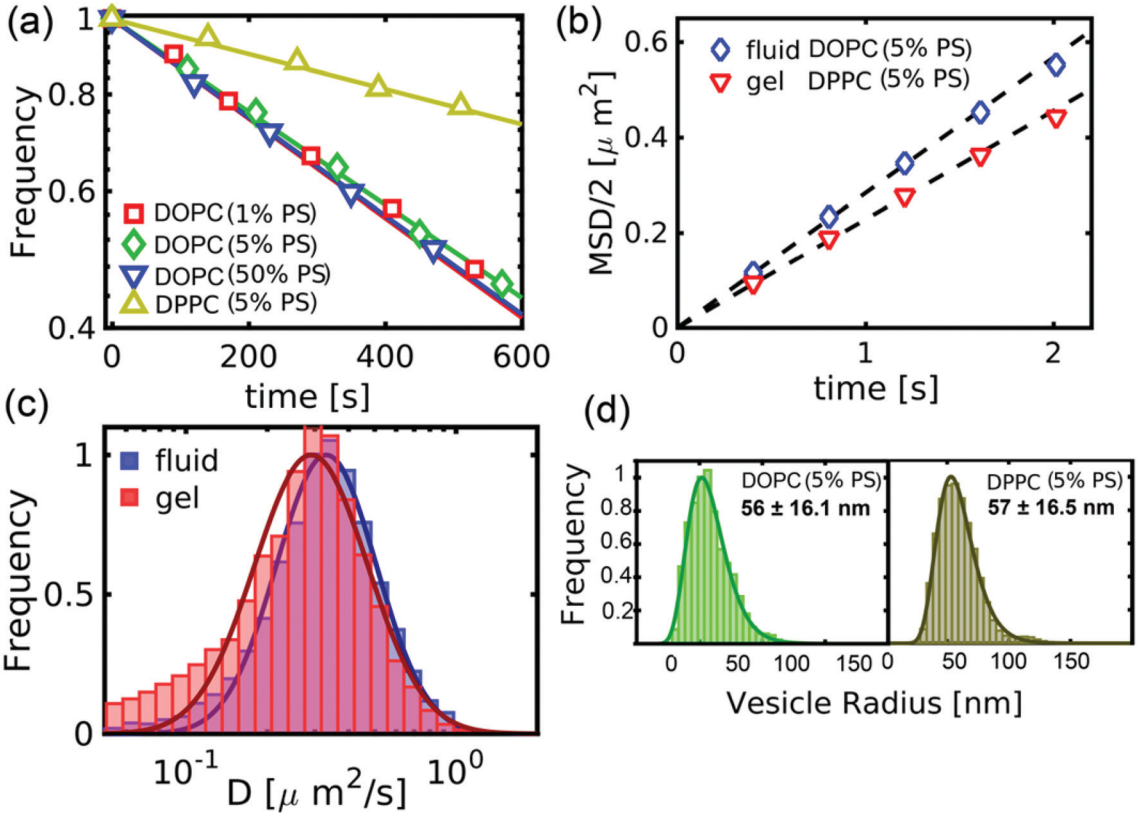

Fig. 3 Kinetics of vesicle detachment from oppositely charged SLB. (a) The number of detected vesicles normalized with the value at $t = 0$ (directly after adsorption), on a logarithmic y-axis, as a function of time for vesicles with various charges and compositions. (b) Half mean squared displacement as a function of elapsed time for fluid phase and gel phase vesicles. The data are the ensemble averages over all vesicles. The slope of the lines, which are fits to the measurement data (markers), equals the SUV diffusivity. (c) Histograms of diffusion coefficients D for gel phase (DOPC) vesicles (red bars) and fluid phase (DOPC) vesicles (blue bars). Note the logarithmic x-axis. (d) Size distribution for DOPC (5% PS) and DOPS (5% PS), measured with the nanoparticle tracking analysis method.

Fig. 3a also shows desorption kinetics for the DPPC vesicles, which are in the gel state. Similar to the fluid phase vesicles, we observe an exponential desorption rate for the gel phase vesicles. The desorption rate for the gel phase vesicles is however substantially smaller than that for the fluid phase vesicles.

To shed light on the origin of this difference, we first verified that the fluid phase (DOPC) and the gel phase (DPPC) vesicles have roughly the same adhesive interaction with the supporting membrane. To this end we have measured the diffusional motion of the membrane adhering vesicles, using single-particle tracking. For this purpose we recorded the trajectories of roughly 200 vesicles over a time period of 600 s by taking frames each 50 ms and matching the detected particle positions of consecutive frames. In Fig. 3b we show that for both vesicles the (ensemble averaged) mean squared displacement (MSD) increases linearly with time, which indicates Brownian diffusion. The computed diffusivity distribution (over the vesicles) is found to be very similar for fluid phase vesicles: $D = 0.28 \pm 0.14\ \mu m^2\ s^{-1}$ as for gel phase vesicles: $D = 0.23 \pm 0.12\ \mu m^2\ s^{-1}$ (Fig. 3c), suggesting that the adhesive interaction with the supported membrane is very similar for the gel phase vesicles as for the fluid phase vesicles. In addition, we verified that the vesicle size distributions of the gel phase [DPPC (5 mol% PS)] and fluid phase [DOPC (5 mol% PS)] vesicles, measured by the Nanoparticle Tracking Analysis (NTA) method,[48] did not differ significantly due to their different lipid compositions (Fig. 3d).

The charge independent, exponential decay, which is shown on a linear y-axis in Fig. 4a, holds an important clue as to the mechanism for the charged lipid transfer that neutralized the electrostatic attraction between the SUV and the SLB, allowing the SUV to desorb from the SLB. This exponential decay suggests that each SUV desorbs, due to a single (or a small number of) stochastic event(s). This view is consistent with stalk formation (Fig. 1c) and subsequent diffusive mixing between the fused leaflets of the opposing membranes, which takes a fraction of a second for nano-sized vesicles. This situation is opposite to the monomer diffusion scenario (depicted in Fig. 1a and b), where there are a large number of independent stochastic events. To contrast this behavior, we plot in Fig. 4a the desorption kinetics corresponding to the monomer diffusion scenario (derived in the ESI†), together with the experimental data. The figure shows that the monomer-

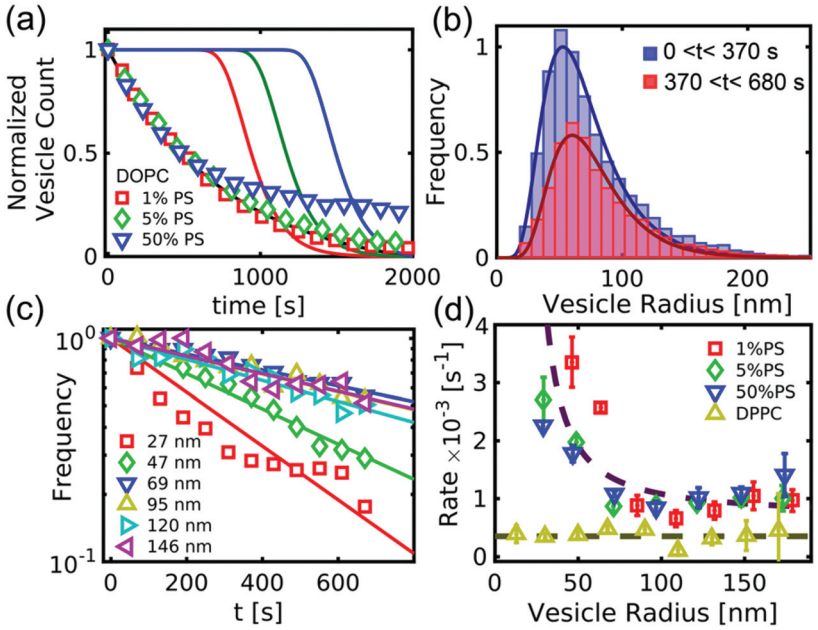

Fig. 4 Effect of vesicle size on the rate of vesicle detachment. (a) The number of detected vesicles normalized with the value at $t = 0$ as a function of time for vesicles of various charge. The experimental data (markers) show a charge independent, exponential decay with no lag-time. The solid lines correspond to a model (derived in the ESI†), that is based on the transfer of individual lipids and predicts a charge dependent lag-time prior to vesicle detachment. The contrast between the experimental data and the model suggests that the vesicles neutralize through a single (or a small number of) stochastic event(s). (b) A typical size distribution of membrane-attached vesicles (5% PS) during an early stage ($0 < t < 370$ s) and a later stage ($370 < t < 680$ s) of the recorded detachment process. The size of individual vesicles is obtained from the fluorescence intensity of a membrane residing dye (rhodamine-PE). (c) The detachment kinetics of vesicles with various sizes on a logarithmic axis, where the vesicle sizes are obtained from the fluorescence intensity. (d) The rate of the vesicle detachment as a function of the size for vesicles with varying charge and composition.

diffusion-driven-desorption-kinetics has a substantial (charge dependent) lag time after adsorption before the vesicles start to desorb. In the ESI† we show that this lag-time is large compared to the decay time, even when there is substantial vesicle charge variation. The experimental data in Fig. 4a, however, show exponential decay, with no (charge dependent) lag time. This discrepancy supports the view that the present desorption mechanism is driven by a single stochastic event, which is consistent with diffusive mixing between fused leaflets due to stalk formation.

Although the hemi-fused state has been hypothesized for nanoscopic vesicles,[43–45] to date no direct evidence has been presented in favor of this. For microscopic vesicles on the other hand, the hemi-fused state has been observed using optical techniques.[15,46]

We continue by analyzing the effect of the membrane curvature (inverse size) on the vesicle desorption process. The size of individual vesicles is measured, through the fluorescence intensity emitted from a dye (rhodamine-PE) residing in the vesicle membrane.[47] Under the assumption of a constant dye concentration (*i.e.* number of dye molecules per area), the intensity is proportional to the vesicle surface area (the size is proportional to the square root of the intensity). A conversion factor is required to translate the square root of the intensity to the vesicle size, which is obtained from the size distribution of the same batch of vesicles, measured using Nanoparticle Tracking Analysis (NTA),[48] (see Materials and methods for detailed analysis).

Fig. 4b shows the resulting size (radius a) distribution $N(a)$, during an early and a later stage of the recorded detachment process for vesicles consisting of 95% DOPC and 5% DOPS lipids, *i.e.* for $0 < t < 370$ s and for $370 < t < 680$ s (see ESI Fig. S2† for $N(a)$ of other vesicles studied). The distributions are well described by log-normal functions (solid lines), which is the usual shape observed for vesicle size distributions.[49] Markedly, the distribution is observed to decay faster for small vesicles than for large ones, indicating a size dependent vesicle detachment rate. To further quantify this size dependence, we plot in Fig. 4c the number of vesicles within different size ranges, as a function of time. Apart from statistical noise, the kinetics of vesicle detachment $[\log(N(a))]$ for various sizes is observed to be a linear function of t, indicating exponential decay.

The size dependent detachment rate $k(a)$ is obtained by fitting $\mathrm{d}N(a)/\mathrm{d}t = -k(a)N(a)$ to the experimental data in Fig. 4c and the result is plotted in Fig. 4d. As anticipated $k(a)$ is a decreasing function of the vesicle radius. In addition there is an additional, curvature-insensitive component, which dominates the detachment rate above a radius of around 100 nm. A similar effect of membrane curvature on lipid exchange has

been reported for cholesterol exchange between vesicles.[50] As the membrane stress in highly curved membranes promotes membrane fusion,[16] the result in Fig. 4d supports our hypothesis that stalk formation and subsequent lipid mixing and not transfer of individual lipids is responsible for the observed detachment of fluid-phase vesicles. For gel phase vesicles on the other hand, lipid mixing *via* stalk formation is not expected, as this mechanism of mixing requires lipid diffusion within the fused leaflets of the opposing membranes, which is inhibited in the gel state. Therefore the observed vesicle desorption for gel phase vesicles is most likely driven by thermal fluctuations that may occasionally kick the SUV away from the SLB, without any lipid transfer, which would also explain the smaller desorption rate, compared to the fluid phase vesicles (Fig. 3a). Fig. 4c also shows that the detachment rate of gel phase vesicles exhibits no curvature dependence, compared to fluid phase vesicles, which again reflects a different mechanism (thermal fluctuations) of desorption for vesicles in the gel phase compared to vesicles in the fluid phase (lipid exchange).

In summary, we have measured the detachment rate of nano-sized lipid vesicles that are electrostatically adhering to a supported lipid membrane. Interestingly, we found that the detachment rate of fluid phase vesicles is independent of the vesicle charge, and it follows an exponential decay. These observations strongly support the view that the vesicle detachment is mediated by charge neutralization due to intermembrane lipid mixing through a single (or few) stochastic event(s), as opposed to many independent events. We therefore hypothesize that the mixing occurs through stalk formation between the opposing membranes and not by diffusion of individual lipids. The observed curvature dependence of the vesicle detachment rate reflects that stalk formation is driven by mechanical energy stored in the curved membrane.[51] For gel phase vesicles on the other hand stalk formation is unlikely, and the desorption is conceived to be driven by thermal fluctuations only, which explains the slower rate and the insensitivity to the curvature. Altogether, the fluorescence microscopy assay employed in this work may open up the possibility to study the statistics of stalk formation in a detailed and controlled manner.

Materials and methods

Small unilamellar vesicle (SUV) preparation

SUVs were prepared by the extrusion method. A chloroform solution of lipids (from Avanti Polar Lipids) with desired composition was first dried using a flow of nitrogen and kept under vacuum for 3 h. The dried lipid film then was rehydrated with an aqueous buffer (10 mM tris, 150 mM NaCl, pH 7.5). The aqueous lipid solution (4 mg ml^{-1}) was vortex mixed, before that vesicles were prepared by using a Mini Extruder (Avanti Polar Lipids) using a polycarbonate membrane with a pore size of 50 and 100 nm.

Supported lipid bilayer formation

SLBs were formed using vesicles composed of 90 mol% DOPC and 10 mol% DOEPC, by injecting vesicles (0.5 mg ml^{-1}) into a rectangular channel with a length, width and height of 50, 5 and 0.1 mm respectively. For all experiments, oxygen plasma-treated glass coverslips (Menzel Gläser, Braunschweig, Germany) were used as the substrate.

Fluorescence recovery after photobleaching (FRAP)

A circular spot (diameter 20 μm) was photobleached with a 100 mW laser beam. The bleaching time was 5 s. The recovery was followed for 5 min by time-lapsed recording of the spatial distribution of the fluorescence intensity in a region of 136 μm by 136 μm, with a 5 s interval. FRAP experimental data were analysed using the Hankel transform method.[42] To label the bilayer, 1% NBD-PE [1,2-dipalmitoyl-*sn-glycero*-3-phosphoethanolamine-*N*-(7-nitro-2-1,3-benzoxadiazol-4-yl) (ammonium salt)] was included in the vesicles that were used to make the bilayer.

Total internal reflection fluorescence (TIRF) microscopy

SUVs on SLB were observed using total internal reflection fluorescence (TIRF) microscopy with an inverted Eclipse TE 2000 microscope (Nikon) equipped with a high-pressure mercury lamp, an Apo TIRF 60× oil objective (NA 1.49), and an Andor iXon+ EMCCD camera (Andor Technology, Belfast, Northern Ireland). The acquired images consisted of 512 × 512 pixels with a pixel size of 0.267 × 0.267 μm. Images were acquired using 200 ms exposure time in time intervals of 20 s for a total time period of 30 min.

Vesicle size determination

Image analysis is conducted in Matlab R2015b. A vesicle is defined as a group of at least three connected pixels exceeding an intensity threshold that was set at 3 times the average noise level. The vesicle intensity is converted to a vesicle size, by assuming that the size is proportional to the square root of the intensity:[47]

$$a = c_{I\to a}\sqrt{I} \quad (1)$$

To obtain the conversion factor $c_{I\to a}$, the same batch of vesicles that was used for microscopy was analyzed by Nanoparticle Tracking Analysis (NTA)[48] using a NanoSight LM10 instrument (NanoSight, Amesbury, UK) (Fig. S3†). As shown in Fig. S2† log-normal distribution functions are fitted to the intensity distribution $N_{\mathrm{TIRF}}(I^{1/2})$, measured with TIRF, and to the size (hydrodynamic radius a) distribution $N_{\mathrm{NTA}}(a)$, measured by NTA. These functions have maximum values at $I_{\mathrm{m}}^{1/2}$ and a_{m}, respectively, and the conversion factor is defined as the ratio of these, *i.e.* $c_{I\to a} = a_{\mathrm{m}}/I_{\mathrm{m}}^{1/2}$.

Vesicle tracking

Vesicle positions in subsequent frames are matched to construct vesicle trajectories. A trajectory is terminated when the vesicle displacement exceeds five pixels or when the vesicle

comes within five pixels of another vesicle. When the separation again exceeds five pixels, a new trajectory is initiated. In order to determine the vesicle diffusivity from the trajectory, we compute the mean squared displacement $\overline{\Delta x^2}$ as a function of the elapsed time t, where Δx can be either a horizontal or a vertical displacement. For particles diffusing with diffusivity D, this quantity evolves as:

$$\overline{\Delta x^2} = 2Dt \quad (2)$$

For each vesicle, the mean squared displacement is fitted to eqn (2), which provides the vesicle diffusivity D. In the analysis we ignore vesicles that are stagnant, *i.e.* when the diffusivity is 100 times smaller than the overall (ensemble averaged) value.

Acknowledgements

The authors wish to acknowledge support from the National Re-search Foundation (NRF-NRFF2011-01 and), the National Medical Research Council (NMRC/CBRG/0005/2012) and Nanyang Technological University to N. J. Cho.

References

1 T. M. Allen and P. R. Cullis, *Science*, 2004, **303**, 1818–1822.
2 V. P. Torchilin, *Nat. Rev. Drug Discovery*, 2005, **4**, 145–160.
3 T. Allen, C. Hansen, F. Martin, C. Redemann and A. Yau-Young, *Biochim. Biophys. Acta, Biomembr.*, 1991, **1066**, 29–36.
4 F. J. Martin, *J. Pharm. Sci.*, 1989, **78**, 181.
5 W. A. Prinz, *Cell*, 2010, **143**, 870–874.
6 A. Toulmay and W. A. Prinz, *Curr. Opin. Cell Biol.*, 2011, **23**, 458–463.
7 H. Sprong, P. van der Sluijs and G. van Meer, *Nat. Rev. Mol. Cell Biol.*, 2001, **2**, 504–513.
8 D. Voelker, *Experientia*, 1990, **46**, 569–579.
9 S. Lev, *Nat. Rev. Mol. Cell Biol.*, 2010, **11**, 739–750.
10 D. G. Rueckert and K. Schmidt, *Chem. Phys. Lipids*, 1990, **56**, 1–20.
11 L. R. McLean and M. C. Phillips, *Biochemistry*, 1981, **20**, 2893–2900.
12 J. W. Nichols and R. E. Pagano, *Biochemistry*, 1981, **20**, 2783–2789.
13 J. D. Jones and T. E. Thompson, *Biochemistry*, 1989, **28**, 129–134.
14 T. Zhu, Z. Jiang and Y. Ma, *Colloids Surf., B*, 2012, **97**, 155–161.
15 G. Lei and R. C. MacDonald, *Biophys. J.*, 2003, **85**, 1585–1599.
16 V. Knecht and S.-J. Marrink, *Biophys. J.*, 2007, **92**, 4254–4261.
17 Y. Kozlovsky and M. M. Kozlov, *Biophys. J.*, 2002, **82**, 882–895.
18 T.-Y. Yoon, B. Okumus, F. Zhang, Y.-K. Shin and T. Ha, *Proc. Natl. Acad. Sci. U. S. A.*, 2006, **103**, 19731–19736.
19 R. F. Brown, *Biochim. Biophys. Acta*, 1992, **1113**, 375–389.
20 A.-L. Bernard, M.-A. Guedeau-Boudeville, L. Jullien and J.-M. Di Meglio, *Langmuir*, 2000, **16**, 6809–6820.
21 R. Parthasarathy, P. A. Cripe and J. T. Groves, *Phys. Rev. Lett.*, 2005, **95**, 048101.
22 E. W. Gomez, N. G. Clack, H.-J. Wu and J. T. Groves, *Soft Matter*, 2009, **5**, 1931–1936.
23 A. R. Sapuri, M. M. Baksh and J. T. Groves, *Langmuir*, 2003, **19**, 1606–1610.
24 T. Kuhl, Y. Guo, J. L. Alderfer, A. D. Berman, D. Leckband, J. Israelachvili and S. W. Hui, *Langmuir*, 1996, **12**, 3003–3014.
25 J. Diao, Z. Su, Y. Ishitsuka, B. Lu, K. S. Lee, Y. Lai, Y.-K. Shin and T. Ha, *Nat. Commun.*, 2010, **1**, 54.
26 G. Ohlsson, S. R. Tabaei, J. Beech, J. Kvassman, U. Johanson, P. Kjellbom, J. O. Tegenfeldt and F. Höök, *Lab Chip*, 2012, **12**, 4635–4643.
27 S. Veshaguri, S. M. Christensen, G. C. Kemmer, G. Ghale, M. P. Møller, C. Lohr, A. L. Christensen, B. H. Justesen, I. L. Jørgensen and J. Schiller, *Science*, 2016, **351**, 1469–1473.
28 S. R. Tabaei, M. Rabe, V. P. Zhdanov, N.-J. Cho and F. Höök, *Nano Lett.*, 2012, **12**, 5719–5725.
29 M. M. Baksh, M. Jaros and J. T. Groves, *Nature*, 2004, **427**, 139–141.
30 N. S. Hatzakis, V. K. Bhatia, J. Larsen, K. L. Madsen, P.-Y. Bolinger, A. H. Kunding, J. Castillo, U. Gether, P. Hedegård and D. Stamou, *Nat. Chem. Biol.*, 2009, **5**, 835–841.
31 M. Rabe, S. R. Tabaei, H. Zetterberg, V. P. Zhdanov and F. Höök, *Angew. Chem., Int. Ed.*, 2015, **54**, 1022–1026.
32 K. Ariga, *ChemNanoMat*, 2016, **2**, 333–343.
33 K. Ariga, K. Minami, M. Ebara and J. Nakanishi, *Polym. J.*, 2016, **48**, 371–389.
34 H. T. McMahon, M. M. Kozlov and S. Martens, *Cell*, 2010, **140**, 601–605.
35 E. Sackmann, *Science*, 1996, **271**, 43–48.
36 E. Rascol, J.-M. Devoisselle and J. Chopineau, *Nanoscale*, 2016, **8**, 4780–4798.
37 M. Rodahl, F. Höök, C. Fredriksson, C. A. Keller, A. Krozer, P. Brzezinski, M. Voinova and B. Kasemo, *Faraday Discuss.*, 1997, **107**, 229–246.
38 J. Homola, *Chem. Rev.*, 2008, **108**, 462–493.
39 J. Zlatanova and K. van Holde, *Mol. Cell*, 2006, **24**, 317–329.
40 T. Kirchhausen, *Nat. Rev. Mol. Cell Biol.*, 2000, **1**, 187–198.
41 R. L. Biltonen and D. Lichtenberg, *Chem. Phys. Lipids*, 1993, **64**, 129–142.
42 P. Jonsson, M. P. Jonsson, J. O. Tegenfeldt and F. Höök, *Biophys. J.*, 2008, **95**, 5334–5348.
43 A. Kunze, S. Svedhem and B. Kasemo, *Langmuir*, 2009, **25**, 5146–5158.
44 A. Kunze, P. Sjövall, B. Kasemo and S. Svedhem, *J. Am. Chem. Soc.*, 2009, **131**, 2450–2451.

45 T. Zhu, Z. Jiang and Y. Ma, *Colloids Surf., B*, 2012, **97**, 155–161.
46 J. Solon, P. Streicher, R. Richter, F. Brochard-Wyart and P. Bassereau, *Proc. Natl. Acad. Sci. U. S. A.*, 2006, **103**, 12382–12387.
47 A. H. Kunding, M. W. Mortensen, S. M. Christensen and D. Stamou, *Biophys. J.*, 2008, **95**, 1176–1188.
48 V. Filipe, A. Hawe and W. Jiskoot, *Pharm. Res.*, 2010, **27**, 796–810.
49 S. Egelhaaf, E. Wehrli, M. Adrian and P. Schurtenberger, *J. Microsc.*, 1996, **184**, 214–228.
50 L. R. McLean and M. C. Phillips, *Biochim. Biophys. Acta, Biomembr.*, 1984, **776**, 21–26.
51 D. P. Siegel, *Biophys. J.*, 1993, **65**, 2124.